Chemical Science

ROYAL SOCIETY OF CHEMISTRY

EDGE ARTICLE

View Article Online
View Journal | View Issue

Cite this: *Chem. Sci.*, 2021, **12**, 10106

All publication charges for this article have been paid for by the Royal Society of Chemistry

Tailoring Lewis/Brønsted acid properties of MOF nodes *via* hydrothermal and solvothermal synthesis: simple approach with exceptional catalytic implications†

Sergio Rojas-Buzo, [a] Benjamin Bohigues,[a] Christian W. Lopes, [b] Débora M. Meira,[cd] Mercedes Boronat, [a] Manuel Moliner *[a] and Avelino Corma *[a]

Received 25th May 2021
Accepted 29th June 2021

DOI: 10.1039/d1sc02833b

rsc.li/chemical-science

The Lewis/Brønsted catalytic properties of the Metal–Organic Framework (MOF) nodes can be tuned by simply controlling the solvent employed in the synthetic procedure. In this work, we demonstrate that Hf-MOF-808 can be prepared from a material with a higher amount of Brønsted acid sites, *via* modulated hydrothermal synthesis, to a material with a higher proportion of unsaturated Hf Lewis acid sites, *via* modulated solvothermal synthesis. The Lewis/Brønsted acid properties of the resultant metallic clusters have been studied by different characterization techniques, including XAS, FTIR and NMR spectroscopies, combined with a DFT study. The different nature of the Hf-MOF-808 materials allows their application as selective catalysts in different target reactions requiring Lewis, Brønsted or Lewis–Brønsted acid pairs.

1. Introduction

Metal–Organic Frameworks (MOFs) are microporous crystalline materials, whose framework is formed by inorganic metallic nodes connected through organic ligands.[1] The high chemical tunability of both components enables the rational design of these materials for selective catalytic applications based on unique structure–activity relationships.[2,3] Fine-tuning of the electronic properties of the metal nodes is a well-stablished design pathway to modulate the catalytic properties of MOF-type materials, which can usually be achieved by modifying the nature of the organic linkers,[4] introducing other metals in the metallic nodes[5,6] or creating coordinatively unsaturated open metal sites.[7,8]

Coordinatively unsaturated open metal sites, either naturally present in MOFs with low connectivity on the metal cluster or associated with missing organic linkers in the MOF framework, can act as selective Lewis acid sites for a wide range of organic transformations.[7,9,10] The generation of these defective sites can be efficiently controlled during the solvothermal synthesis of MOFs using modulators, such as monocarboxylic acids or inorganic acids that compete with the organic linkers in bonding to the metallic nodes,[11,12] or following post-synthetic treatments into preformed MOFs, such as acid/base treatments.[8,13] Interestingly, it has been recently reported that the post-incorporation in these defective sites of water molecules *via* hydration processes could facilitate the creation of Brønsted acid sites.[14,15]

Zr- and Hf-MOFs have attracted great attention for their inherent chemical, mechanical and hydrothermal stabilities, offering excellent properties for their wide application in different relevant catalytic processes.[16–20] Despite Hf and Zr should have similar physicochemical properties, the higher oxophilicity of Hf with respect to Zr, should imply a stronger Brønsted acidic character of the μ3-OH groups present on the metallic node.[21,22] However, traditional solvothermal synthesis of Hf-MOFs usually ends up with amorphous materials or requires several weeks to crystallize.[23] For this reason, an alternative modulated hydrothermal approach has been recently applied to successfully synthesize the 12-connected UiO-66 material and the 6-connected MOF-808, both with Zr- and Hf-composition.[24–27] It is worth noting that traditional solvothermal processes require the use of large amounts of organic solvents, preferentially *N*,*N*-dimethylformamide (DMF), which is toxic, flammable and carcinogenic. Thus, these hydrothermally-mediated synthesis methods can be considered

[a]*Instituto de Tecnología Química, Universitat Politècnica de València - Consejo Superior de Investigaciones Científicas, Av. de los Naranjos, s/n, 46022 Valencia, Spain*
[b]*Institute of Chemistry, Universidade Federal do Rio Grande do Sul – UFRGS, Av. Bento Gonçalves, 9500, 91501-970 Porto Alegre, RS, Brazil*
[c]*CLS@APS, Advanced Photon Source, Argonne National Laboratory, 9700 S. Cass Avenue, Argonne, IL 60439, USA*
[d]*Canadian Light Source Inc., 44 Innovation Boulevard, Saskatoon, Saskatchewan S7N 2V3, Canada*

† Electronic supplementary information (ESI) available. See DOI: 10.1039/d1sc02833b

as substantial advances in MOF-type preparation, allowing their synthesis following an environmental-friendly pathway that can undoubtedly facilitate their scale-up preparation.

Herein, we demonstrate that the hydrothermal synthesis of MOFs, in particular Hf-MOF-808, could not only be considered as a green approach to prepare MOFs, but also a plausible and simple synthesis methodology to *in situ* generate Brønsted acid sites in the metal nodes during the synthetic procedure. Furthermore, we will show that the Lewis/Brønsted acid properties of Hf-MOF-808 materials can be easily controlled by performing their preparation *via* modulated solvothermal or hydrothermal synthesis. The different nature of the acid sites generated with each synthesis procedure has been revealed by FTIR and ^{31}P MAS NMR spectroscopies using labelled acetonitrile (CD_3CN) and trimethyl phosphine oxide (TMPO) as probe molecules, respectively, combined with DFT calculations. In addition, XAS spectroscopy has been employed to unravel the electronic properties of the Hf clusters in the two Hf-MOF-808 samples. Finally, the two resultant Hf-MOF-808 materials have been applied in different target reactions requiring Lewis and/or Brønsted acidities, giving clear differences in activity and product selectivity.

2. Experimental section

2.1. Hf-based metal–organic synthetic procedures

2.1.1. Modulated hydrothermal synthesis of Hf-MOF-808. This synthesis has been carried out following a previously reported recipe but using Hf instead of Zr:[28] H_3BTC (1,3,5-benzenetricarboxylic acid) (1.20 mmol, 0.25 g) and $HfOCl_2 \cdot 8H_2O$ (3.63 mmol, 1.49 g) were dissolved in a mixture of H_2O/acetic acid (1 : 1 v/v, 20 mL). The resulting solution was refluxed at 100 °C under magnetic stirring during 37 h. The white precipitate was washed three times with H_2O, three times with methanol and, finally, with acetone. The obtained white solid, denoted as Hf-MOF-808_H_2O, was activated at 100 °C for 2 h (1.09 g, 3.24 mmol, 90.8% yield referred to $HfOCl_2 \cdot 8H_2O$).

2.1.2. Modulated solvothermal synthesis of Hf-MOF-808. This material has been synthesized according to previously reported procedures:[29,30] H_3BTC (1,3,5-benzenetricarboxylic acid) (3.00 mmol, 0.63 g) and $HfCl_4$ (3.00 mmol, 0.96 g) were dissolved in a mixture of DMF/formic acid (1 : 1 v/v, 90 mL). The resulting solution was refluxed at 100 °C under magnetic stirring for two weeks. The precipitate was washed three times with DMF and acetone. The obtained white solid, denoted as Hf-MOF-808_DMF, was activated at 100 °C for 2 h (0.78 g, 2.48 mmol, 82.5% yield referred to $HfCl_4$).

2.2. Characterization

2.2.1. General characterization techniques. Powder X-ray diffraction (PXRD) measurements were performed using a Panalytical CubiX diffractometer operating at 40 kV and 35 mA, and using Cu Kα radiation ($\lambda = 0.1542$ nm).

Chemical analyses were carried out in a Varian 715-ES ICP-Optical Emission spectrometer, after solid dissolution in H_2SO_4/H_2O_2 aqueous solution. Elemental analyses were performed by combustion analysis using a Eurovector EA 3000 CHNS analyzer and sulphanilamide as reference.

The morphology of the samples was studied by field emission scanning electron microscopy (FESEM) using a ZEISS Ultra-55 microscope.

The adsorption and desorption curve of N_2 was measured at 77 K in an ASAP2420 Micromeritics device. The specific surface areas were calculated by the Brunauer–Emmet–Teller (BET) method following Rouquerol's criterion.

Thermogravimetric and thermal differential analysis (TG-DTG) were conducted in air stream with a NETZSCH STA 449F3 STA449F3A-1625-M analyzer (temperature ramp: 25 °C/10.0 (°C/min))/800 °C).

Infrared (FTIR) spectra were recorded in a PIS 100 spectrometer. The solid samples, mixed with KBr, were pressed into a pellet.

2.2.2. FTIR analysis of acetonitrile-d_3 (CD_3CN) adsorption. The Hf-MOF-808 samples were pressed into self-supported wafers and treated at 150 °C in vacuum (10^{-4} mbar) for 1.5 h. After activation, the samples were cooled down to 25 °C. Then, CD_3CN was introduced to the cell until saturation, followed by evacuation under vacuum for 1 h at room temperature.

IR spectra were recorded with a Thermo is50 FTIR spectrometer using a DTGS detector and acquiring at 4 cm^{-1} resolution. A homemade quartz IR cell allowing *in situ* treatments in controlled atmospheres and temperatures from 25 to 525 °C has been connected to a vacuum system with a gas dosing facility.

2.2.3. ^{31}P MAS NMR characterization. Hf-MOF-808 materials (100 mg) were degassed under vacuum at 150 °C for 4 h in a sealed glass sample tube with a stopcock to remove any physisorbed molecules. Samples were thereafter handled under dry nitrogen conditions in a glovebox to prevent exposing them to moisture that can bind to both Hf sites and trimethylphosphine oxide (TMPO). A 0.01 M TMPO solution in dichloromethane (DCM) was prepared. Then, the corresponding amount of the TMPO solution was added to the glass vials containing the materials to obtain the desired TMPO/Hf ratio (~0.20 TMPO/Hf). The resulting mixture was magnetically stirred in the glovebox overnight at room temperature. DCM solvent was removed at 80 °C under vacuum. Finally, the samples were characterized by solid-state ^{31}P MAS NMR spectroscopy.

Solid-state ^{31}P MAS NMR spectra were recorded at room temperature under magic angle spinning (MAS) in a Brucker AV-400 spectrometer at 161.9 MHz with a spinning rate of 10 kHz and $\pi/2$ pulse length of 3.7 μs with spinal proton decoupling and recycle delay of 20 s. ^{31}P chemical shift was referred to phosphoric acid.

2.2.4. XPS measurements. X-ray photoelectron spectra were collected using a SPECS spectrometer with a 150 MCD-9 detector and using a non-monochromatic MgKα (1253.6 eV) X-ray source. Spectra were recorded using analyzer pass energy of 30 eV, an X-ray power of 50 W and under an operating pressure of 10^{-9} mbar. During data processing of the XPS spectra, binding energy (BE) values were referenced to C 1s peak (284.8 eV). Spectra treatment has been performed using the CASA software.

2.2.5. XAS spectroscopy study. X-ray absorption spectroscopy experiments were carried out at the Hf L_3-edge (9561 eV) using the 20 BM beamline of Argonne National Laboratory (Lemont, IL, USA).[31] The samples were pelletized and the spectra were collected at room temperature in transmission mode using ionization chambers as detectors. Zn foil placed between I1 and I2 ionization chambers was used for energy calibration. Several scans per sample were acquired to ensure spectral reproducibility and good signal-to-noise ratio. Data reduction and extraction of the $\chi(k)$ functions were performed using Athena software while EXAFS data analysis was done with Artemis software, as implemented in the Demeter package.[32] A corefinement approach of data fitting was adopted, using two Debye–Waller factors (σ^2) per spectrum and the same energy threshold (E_0) for both samples. The σ^2 and E_0 values were let to vary during the fit but common between the spectra. Phase and amplitudes have been calculated by FEFF6 code using orthorhombic hafnia crystallographic file as input. Additional information will be displayed as a note below the table of EXAFS results.

2.3. DFT simulations

All density functional theory (DFT) calculations were carried out using the M062X functional,[33] the 6-31g(d,p) basis set for O, C, P and H atoms,[34,35] and the LANL2DZ basis set and pseudopotential for Hf[36,37] as implemented in the Gaussian 09 software.[38] For the simulation of NMR parameters, the isotropic absolute chemical shielding constants (σ) were obtained using the gauge including atomic orbitals (GIAO) approach[39,40] and the ^{31}P chemical shifts were calculated as $\delta_{iso}(^{31}P) = \sigma_{ref} - \sigma$, using phosphoric acid as reference. To improve accuracy, all values were corrected with an equation obtained by fitting $\delta_{iso}(^{31}P)$ values at 6-31G(d,p) level against $\delta_{iso}(^{31}P)$ values at 6-311++G(d,p) level for a series of acid–base TMPO adducts, described in reference [41].

The active sites present in the Hf-MOF-808 were simulated by cluster models containing one $[Hf_6O_4(OH)_4]^{12+}$ node, the first shell of six organic linkers surrounding it, extracted from the experimental structure MOF-808,[29] and the six hydroxyl groups necessary to compensate the excess positive charge (see Fig. S1†). The organic linkers were simulated by benzoate anions in which the carboxylic groups of the linkers not bonded to the $[Hf_6O_4(OH)_4]^{12+}$ node were replaced by hydrogen atoms. In a first step, all C–H distances were optimized while keeping the positions of all other atoms in the model fixed, and in the subsequent geometry optimizations the five hydrogen atoms of each benzoate group were kept fixed at these optimized positions in order to maintain the structure of the MOF while all other atoms in the system were allowed to move without restrictions. Models A and B in Fig. S1† include a first shell of water molecules strongly coordinated to the Hf atoms and hydrogen bonded to the hydroxyl groups, while in models C and D this shell of stabilizing water was removed to simulate the possible desorption of some of these water molecules due to the pre-treatment of the samples prior to the ^{31}P MAS NMR experiments. Models B and D are generated by proton transfer from a μ3-OH Brønsted acid site (dotted circles in Fig. S1†) to a neighboring carboxylic group. The network of water molecules in B stabilize this proton, making this migration 10 kcal mol^{-1} more favorable than the same process in the dehydrated D system. Additional water molecules are included in models E to H to simulate possible structures favored in the hydrothermal synthesis, including the partial displacement of one carboxylate linker in structure F.

2.4. Catalytic test reactions

2.4.1. Meerwein–Ponndorf–Verley reduction of acetophenone with isopropanol. The Meerwein–Ponndorf–Verley reactions were performed in 2 mL glass-vessel reactors equipped with a magnetic bar. Acetophenone (0.45 mmol, 54 mg), dodecane (0.22 mmol, 37.40 mg) as external standard and isopropanol (1.6 mL) were added to each reactor containing the corresponding amount of Hf-MOF-808 (10 mol% Hf). The mixtures were placed in an aluminum heating block at 100 °C with magnetic stirring. Approximately 50 μL aliquots were taken at different times, diluted with ethyl acetate and centrifuged. The supernatant obtained from batch reactions were analyzed using gas chromatography in an instrument equipped with a 25 m capillary column of 5% phenylmethylsilicone.

2.4.2. Styrene oxide ring-opening with isopropanol. The epoxide ring-opening reactions were performed in 2 mL glass-vessel reactors equipped with a magnetic bar. Styrene oxide (0.75 mmol, 90.10 mg), *o*-xylene (0.21 mmol, 22.50 mg) as external standard and isopropanol (2 mL) were added to each reactor containing the corresponding amount of Hf-MOF-808 (2.5 mol% Hf). The mixtures were placed in an aluminum heating block at 55 °C with magnetic stirring. Approximately 50 μL aliquots were taken at different times, diluted with ethyl acetate and centrifuged. The supernatant obtained from batch reactions were analyzed using gas chromatography in an instrument equipped with a 25 m capillary column of 5% phenylmethylsilicone.

2.4.3. α-Pinene oxide isomerization. The isomerization reactions were performed in 2 mL glass-vessel reactors equipped with a magnetic bar. α-Pinene oxide (0.34 mmol, 52 mg), dodecane (0.30 mmol, 51.10 mg) as external standard and toluene (2 mL) were added to each reactor containing the corresponding amount of Hf-MOF-808 (10 mol% Hf). The mixtures were placed in an aluminum heating block at 70 °C with magnetic stirring. Approximately 50 μL aliquots were taken at different times, diluted with ethyl acetate and centrifuged. The supernatant obtained from batch reactions were analyzed using gas chromatography in an instrument equipped with a 25 m capillary column of 5% phenylmethylsilicone.

3. Results and discussion

3.1. Synthesis and characterization of materials

The Hf-MOF-808 material prepared *via* modulated hydrothermal synthesis, denoted as Hf-MOF-808_H_2O, requires less time to crystallize than the Hf-MOF-808 prepared *via* modulated solvothermal synthesis, denoted Hf-MOF-808_DMF (see

synthesis details in Experimental section). Both samples show the formation of the MOF-808 structure as pure crystalline phase (see PXRD patterns in Fig. 1), and analogous crystal sizes (~400 nm, see Fig. 2).

Moreover, the nitrogen adsorption measurements reveal similar textural properties for both Hf-MOF-808 materials (see Fig. S2†), with a micropore volume and micropore area of ~0.52–0.54 $cm^3\ g^{-1}$ and 1065–1094 $m^2\ g^{-1}$, respectively (see Table 1). The FTIR spectra of both materials clearly show the shift of the ~1717 cm^{-1} signal, assigned to the carbonyl stretch C=O of the free carboxylic acid group of trimesic acid (see Fig. S3†), indicating the entire interaction of the organic ligand with the Hafnium clusters. The chemical composition of both materials is also similar, presenting a ~33–36% wt Hf (see Table 1), which could also be corroborated by thermogravimetric analysis (see Fig. S4†), where the organic linker decomposes up to 350 °C.

3.2. Lewis and Brønsted acid-sites characterization

The nature and relative amount of the acid sites present in the MOF-808 samples have been studied by FTIR and ^{31}P MAS NMR spectroscopy using CD_3CN and TMPO as probe molecules, respectively. CD_3CN chemisorption monitored by FTIR spectroscopy allows identifying the nature of the acid sites in the Hf-MOF-808 materials (see details in Experimental section). Fig. 3 shows three principal ν(CN) vibrational bands at 2307–2311, 2272 and 2261 cm^{-1}, assigned to the CD_3CN adsorption on Lewis and Brønsted acid sites and physisorbed acetonitrile, respectively.[42–44] The relative ratio between the integrated signals associated with Brønsted and Lewis acid sites (band centered at 2272 and 2307–2311 cm^{-1}, respectively) is at least two times higher for the Hf-MOF-808_H_2O sample than for the Hf-MOF-808_DMF sample under the conditions employed for the CD_3CN-FTIR spectroscopy experiment. This characterization clearly suggests that the Brønsted acidity increases through the introduction of OH groups on the metallic nodes during the hydrothermal synthesis.

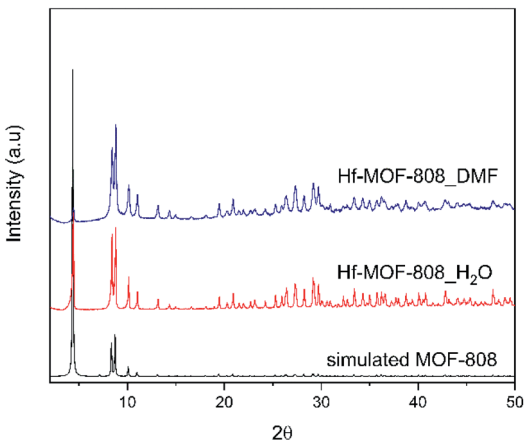

Fig. 1 Experimental and simulated PXRD patterns of Hf-MOF-808_H_2O (red line) and Hf-MOF-808_DMF (blue line).

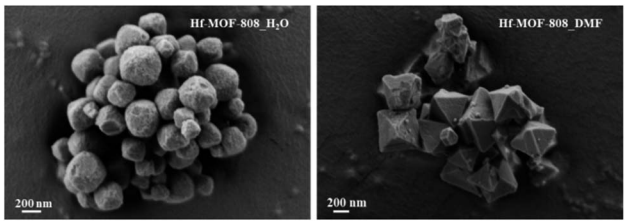

Fig. 2 SEM images for Hf-MOF-808_H_2O and Hf-MOF-808_DMF.

On the other hand, TMPO is a probe molecule that can diffuse through the MOF-808 pores and interact with both Lewis and Brønsted acid sites present in the metal-containing nodes, so the two types of acid sites can be distinguished by analysis of the ^{31}P MAS NMR spectra after TMPO adsorption.[41,45,46] Indeed, clear differences are observed between the ^{31}P MAS NMR spectra of the two TMPO-adsorbed Hf-MOF-808 samples (see Fig. 4). The contribution of the signals between 55 and 58 ppm, which have been recently assigned to the interaction of TMPO with Zr Lewis acid sites in UiO-66(Zr) and Zr-MOF-808,[41] is considerably higher in the MOF-808 sample obtained *via* solvothermal synthesis (see Table S1†). Moreover, the proportion of the components at 62 and 68 ppm, which have been previously related to TMPO interacting with Brønsted acid sites in sulfated Zr-MOF-808,[47] is higher in the sample obtained *via* hydrothermal synthesis (see Table S1†). These results also corroborate that the relative amount of Brønsted to Lewis acid sites is remarkably higher in the Hf-MOF-808_H_2O. To confirm the assignation of the peaks in the case of the Hf-containing MOF-808, and in an attempt to clarify the origin of the differences between the two MOF-808 samples, the isotropic $\delta(^{31}P)$ chemical shifts of TMPO interacting with some hydrated and dehydrated catalyst models depicted in Fig. S1† were simulated by means of DFT calculations.

In agreement with previous assignations for Zr-containing MOFs,[41] the $\delta(^{31}P)$ chemical shift calculated for TMPO interacting with Hf Lewis acid sites is 52 ppm (see Table S2† and Fig. 5), while the values obtained for the weaker interaction with μ3-OH Brønsted acid sites are slightly lower, 48 ppm. Additional water molecules, even if they are placed in such a way that the carboxylic group of the linker is partly de-coordinated as in structure E, are not able to protonate TMPO and the calculated $\delta(^{31}P)$ shifts are 42–43 ppm, not observed experimentally. However, a $\delta(^{31}P)$ value of 68 ppm is obtained for protonated TMPO interacting with Hf-MOF-808, in a system in where the proton comes from a μ3-OH acid site (structure B in Fig. 5). The proton migration that converts A into B is facilitated by the network of water molecules coordinated or surrounding the Hf node, which are probably more abundant in the hydrothermal synthesis and would explain the much higher intensity of the peak at 62 ppm in the Hf-MOF-808_H_2O sample. These results confirm that the proportion of Lewis to Brønsted acid sites is remarkably higher in the Hf-MOF-808_DMF, while the trend is the opposite in the Hf-MOF-808_H_2O.

XPS and XAS spectroscopy has been used to evaluate the electronic properties of the Hf clusters in the Hf-MOF-808

Table 1 Data characterizing the MOF-808 materials: chemical composition, N_2 adsorption isotherms and catalytic performance for the Meerwein–Ponndorf–Verley (MPV) and the epoxide ring-opening (ERO) reactions

	Chemical composition				N_2 adsorption isotherms			Catalytic performance[c]	
Sample	Hf[a] (% wt)	C[b] (% wt)	H[b] (% wt)	N[b] (% wt)	BET surf. area ($m^2\ g^{-1}$)	Microp. area ($m^2\ g^{-1}$)	Microp. vol. ($cm^3\ g^{-1}$)	MPV[d]	ERO[e]
Hf-MOF-808 H_2O	33.6	11.2	2.7	—	1123	1065	0.52	1.23	5.42
Hf-MOF-808 DMF	36.2	17.9	2.1	2.1	1135	1094	0.54	6.05	2.55

[a] Measured by ICP analysis. [b] Measured by elemental analysis. [c] Determinated by TOF values (h^{-1}). Reaction conditions. [d] Acetophenone (0.45 mmol), isopropanol (1.6 mL), and MOF catalyst (10 mol% Hf), temperature 100 °C. [e] Styrene oxide (0.75 mmol), isopropanol (2 mL), and MOF catalyst (2.5 mol% Hf), temperature 55 °C.

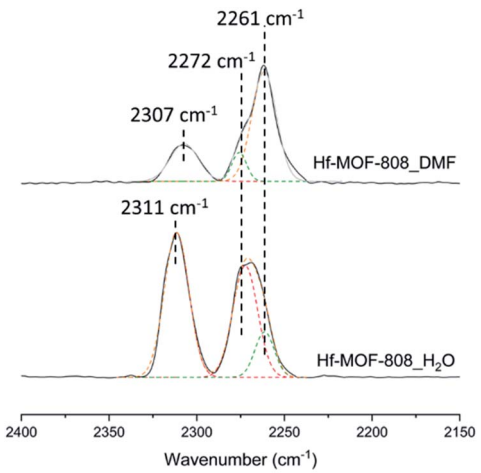

Fig. 3 FTIR spectra of 2 mbar CD_3CN adsorbed at 25 °C on Hf-MOF-808_H_2O (down) and Hf-MOF-808_DMF (top). The IR bands at 2311 and 2307 cm^{-1} are associated with CD_3CN coordinated to Hf sites, and the IR bands at 2272 cm^{-1} to OH groups in the Hf cluster. The band at 2261 cm^{-1} is associated with physisorbed CD_3CN molecules.

samples. In both Hf-MOFs, the Hf4f core line in the XPS spectra contains two peaks at 17.6 and 19.2 binding energy, corresponding to the $Hf4f_{5/2}$ and $Hf4f_{7/2}$ components of hafnium in the oxidation state Hf^{4+} (see Fig. S5†).[48,49] On the other hand, the normalized XANES spectra at Hf L_3-edge of the Hf-MOF-808_DMF, Hf-MOF-808_H_2O and Hf-based standards are shown in Fig. 6. In both MOF samples, Hf^{4+} is the main oxidation state due to the position of the first derivative at ~9563 eV,[50,51] corroborating the results obtained in the XPS analysis. The intense whiteline (related to the $2p_{3/2} \rightarrow 5d$ electronic transition) of the MOFs is similar to that of other Hf-based materials,[50] which is stronger in the Hf-MOF-808_DMF followed by the Hf-MOF-808_H_2O sample. EXAFS data (see Table S3 and Fig. S6†) indicate a similar local environment around Hf atoms in both samples, with each Hf atom interacting with approximately six nearest neighbours (averaging of oxygen atoms in the metal cluster and/or solvent molecules). The obtained Hf–O and Hf–Hf distances lie between those obtained by Gianolio *et al.*[52] for hydroxylated/dehydroxilated Hf-MOFs.

3.3. Catalytic activity: Lewis and Brønsted acid-sites

After unraveling the different nature of the metallic nodes of the above described Hf-MOF-808 materials, two different catalytic processes requiring Lewis and Brønsted acid sites, such as the Meerwein–Ponndorf–Verley (MPV) and the epoxide ring-opening (ERO) reactions, respectively, have been tested to evaluate their catalytic performance. The Meerwein–Ponndorf–Verley reduction of carbonyl compounds with alcohols has been described as a model reaction to study the Lewis acidity in Hf-MOFs (see Scheme 1).[53–55] For this reason, the Hf-MOF-808 materials synthesized in this work are first tested for the MPV reaction of acetophenone and isopropanol (see the Experimental section for details). While the acetophenone conversion reaches ~90% after 6 h when Hf-MOF-808_DMF is used as catalyst, the acetophenone conversion only achieves ~64% after 6 h with Hf-MOF-808_H_2O (see Fig. 7). The calculated turnover

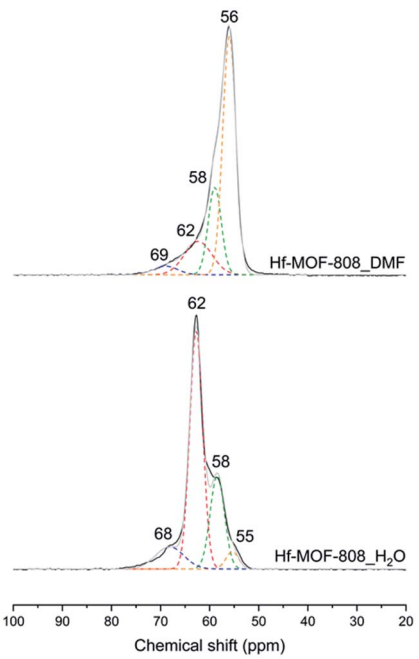

Fig. 4 ^{31}P MAS NMR spectra of TMPO loaded on Hf-MOF-808_H_2O (down) and Hf-MOF-808_DMF (top). Experimental spectra are shown in black and the sum of the deconvoluted peaks in gray.

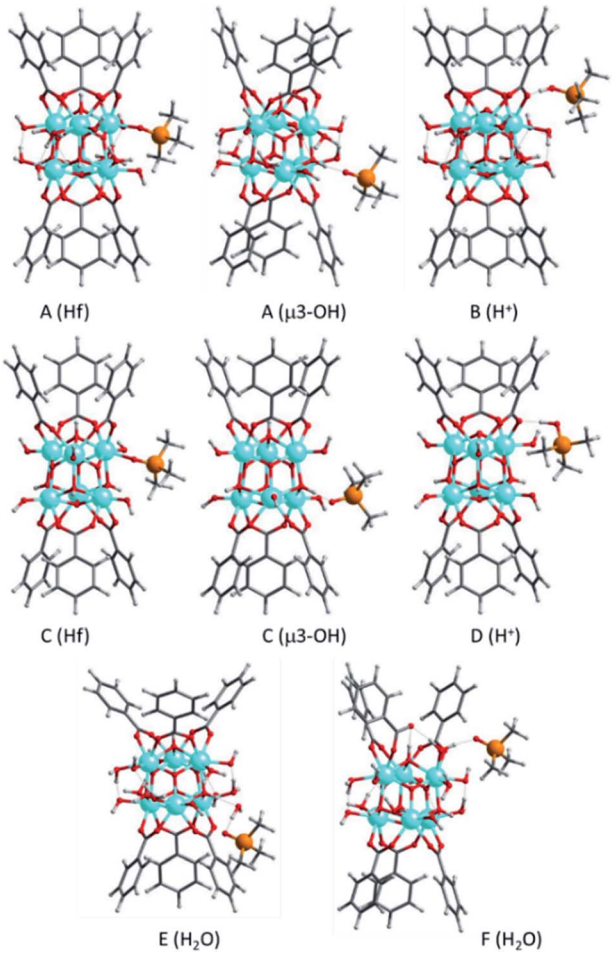

Fig. 5 Optimized geometries of TMPO interacting with Hf Lewis sites, μ3-OH Brønsted acid sites, or additional H_2O molecules, and of protonated $TMPOH^+$ in Hf-MOF-808 models. The labels A to F identify the MOF-808 model used, as described in Fig. S1,† and the type of interaction between TMPO and MOF-808 is given in parenthesis. C and O atoms are depicted as gray and red sticks, Hf, P and H as cyan, yellow and white balls.

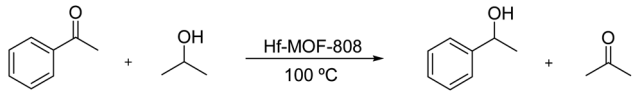

Scheme 1 Meerwein–Ponndorf–Verley reduction of acetophenone with isopropanol catalyzed by Hf-MOF-808.

frequency (TOF) with Hf-MOF-808_DMF is ~5.0 times higher than the calculated TOF when using Hf-MOF-808_H_2O for the MPV transformation (see Table 1). This result is consistent with the previous characterization. The higher amount of 5d orbitals in the MOF-808 sample synthesized in DMF media and, therefore, the more accessible Lewis acid sites, would corroborate its higher activity for the Lewis acid-demanding MPV catalytic reaction.

On the other hand, the oxide ring-opening reaction (see Scheme 2) has been employed as a model catalytic test to distinguish catalytic Brønsted acid sites.[16,56,57] Considering this, Hf-MOF-808_H_2O and Hf-MOF-808_DMF have been tested for the styrene oxide ring-opening reaction with isopropanol (see the experimental section for details).

The styrene oxide conversion is almost completed after 21 h when using Hf-MOF-808_H_2O as catalyst, whereas Hf-MOF-808_DMF material only achieves ~43% conversion at this point (see Fig. 8). Moreover, the calculated TOF (h^{-1}) with Hf-MOF-808_H_2O catalyst is ~2.0 higher than Hf-MOF-808_DMF for this transformation (see Table 1). The improved Brønsted acidity introduced into the metallic nodes of the Hf-MOF-808 during the hydrothermal synthesis would explain the remarkable catalytic differences for the styrene ring-opening reaction.

If both reactions are considered, the relative catalytic activities, measured as TOF_{ERO}/TOF_{MPV}, for Hf-MOF-808_H_2O and Hf-MOF-808_DMF are 4.41 and 0.42, respectively (see Table S1†). The different relative catalytic activity by a factor of ~10 for the two Hf-MOF-808 catalysts, could be tentatively connected to the different relative amount of Brønsted to Lewis acid sites obtained from the ^{31}P MAS NMR spectra after TMPO

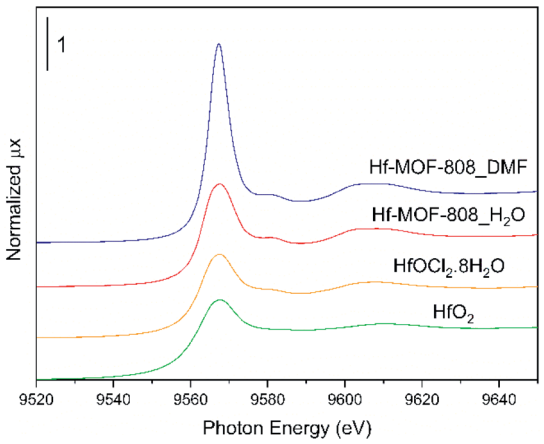

Fig. 6 Normalized XANES spectra at Hf L_3-edge of Hf-MOF-808 samples and Hf-based standards.

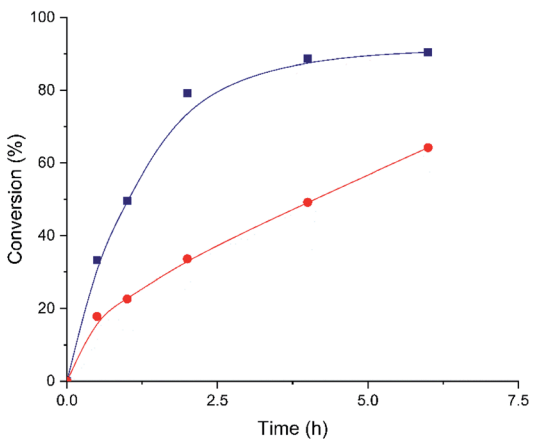

Fig. 7 Kinetic profiles for acetophenone conversion employing Hf-MOF-808_H_2O (red circles) and Hf-MOF-808_DMF (blue squares) as catalysts.

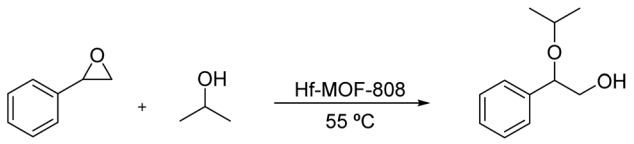

Scheme 2 Styrene oxide ring-opening with isopropanol catalyzed by Hf-MOF-808.

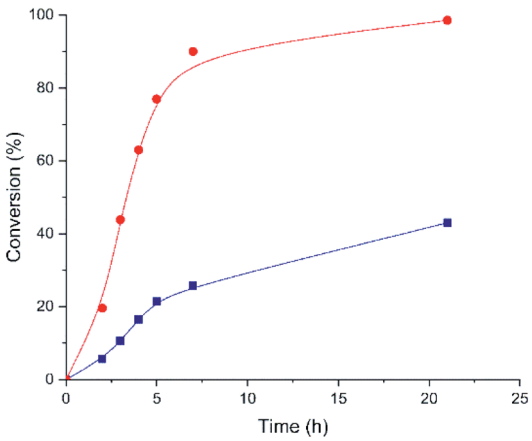

Fig. 8 Kinetic profiles for styrene oxide conversion employing Hf-MOF-808_H_2O (red circles) and Hf-MOF-808_DMF (blue squares) as catalysts.

adsorption, which is ~9 times higher for Hf-MOF-808_H_2O than for Hf-MOF-808_DMF (see Table S1†). These evidences may indicate good structure–activity relationships for both Hf-containing MOF-808 catalysts.

Finally, the α-pinene oxide isomerization has been employed to evaluate the catalytic performance of the prepared Hf-MOF-808, since this reaction is very sensitive to the presence of Lewis and Brønsted acid sites. Indeed, the product distribution of this reaction unavoidably depends on the nature of the acid sites (see Scheme 3): (1) the selectivity toward campholenic aldehyde (CA) is usually lower than 55% with Brønsted acids, whereas the CA selectivity is considerably higher with Lewis acid sites (>85%);[58,59] (2) a significant amount of *trans*-carveol is formed with Brønsted acid sites.[60–62]

As seen in Fig. 9 and S7,† both Hf-MOF-808 materials show a similar α-pinene oxide conversion after 5 h (~75–80%), but the product distribution is considerably different. Hf-MOF-808 obtained *via* hydrothermal synthesis shows ~45% selectivity toward CA, in good agreement with descriptions in the literature where Brønsted acid catalysts present CA selectivities below 55% (see Fig. 9 and S8†), whereas Lewis-acid containing Hf-

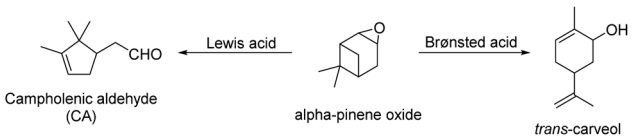

Scheme 3 Isomerization of α-pinene oxide.

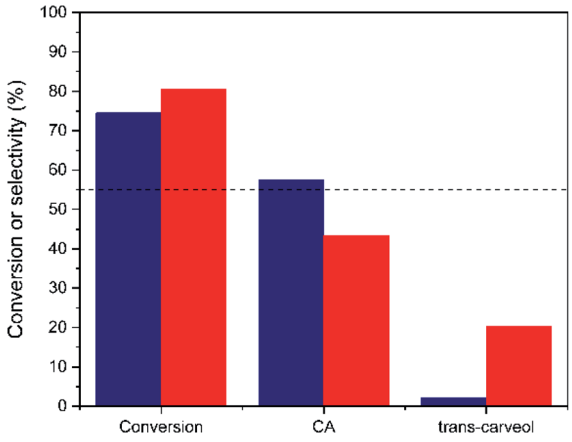

Fig. 9 Conversion and different product selectivities obtained for the α-pinene oxide isomerization when using Hf-MOF-808_H_2O (red bar) and Hf-MOF-808_DMF (blue bar) as catalysts.

MOF-808_DMF approaches ~60% CA selectivity (see blue bar in Fig. 9). Moreover, a remarkably higher amount of *trans*-carveol has been obtained when using the Hf-MOF-808_H_2O as catalyst (~20%, see Fig. 9) compared to Hf-MOF-808_DMF, where only traces of *trans*-carveol are observed (see Fig. 9).

The heterogeneous catalytic nature and the cycle performance of the Hf-MOFs for the α-pinene oxide isomerization have been studied. To do this, hot filtration and recyclability tests have been carried out, respectively (see Fig. S9†). On the one hand, the α-pinene oxide conversions remain unaltered after filtering the solid catalysts in both cases (see Fig. S9A†). On the other hand, the Hf-MOF-808 samples can be reused at least two consecutive runs with only a minor decrease in the catalytic activity (see Fig. S9B†). These evidences corroborate the heterogeneous catalytic nature and the stability of the Hf-MOF-808 catalysts for the α-pinene oxide isomerization reaction.

4. Conclusions

In this work, it has been shown how the Lewis/Brønsted catalytic properties of the Hf-MOF-808 material can be simply and efficiently adjusted by controlling the solvent employed in the synthetic procedure. The modulated hydrothermal synthesis maximizes the presence of Brønsted acid sites, whereas solvothermal synthesis allows increasing the proportion of unsaturated Hf Lewis acid sites. These different Lewis/Brønsted acidities, which have been adequately characterized by different techniques, in Hf-MOF-808 materials have a direct impact on their catalytic activity and selectivity, in particular when very sensitive and complex target reactions are studied. The ability to design and control the different nature of the metallic active sites by simple, direct and green synthesis methods, as those presented here for the Hf-MOF-808 material, could be extended to other MOF-type structures and even to the design of multifunctional MOF-based catalysts where different metals or organic linkers can be combined to incorporate other chemical functionalities.

Author contributions

The manuscript was written through the contributions of all authors. All authors have given approval to the final version of the manuscript.

Conflicts of interest

There are no conflicts to declare.

Acknowledgements

This work has been supported by the Spanish Government through the "Severo Ochoa" (SEV-2016-0683, MINECO), MAT2017-82288-C2-1-P (AEI/FEDER, UE) and RTI2018-101033-B-I00 (MCIU/AEI/FEDER, UE). J. M. Salas is acknowledged for his contribution to CD_3CN-FTIR experiments. C. W. L. thanks the PRH 50.1 – ANP/FINEP Human Resources Program for the Visiting Researcher Fellowship. This research used resources of the Advanced Photon Source, a user facility operated for the U.S. Department of Energy (DOE) Office of Science by Argonne National Laboratory, and was supported by the U.S. DOE under Contract No. DE-AC02-06CH11357 and by the Canadian Light Source and its funding partners. The Electron Microscopy Service of the UPV is also acknowledged for their help in sample characterization.

Notes and references

1 H. Furukawa, K. E. Cordova, M. O'Keeffe and O. M. Yaghi, The Chemistry and Applications of Metal-Organic Frameworks, *Science*, 2013, **341**(6149), 1230444.

2 A. Corma, Heterogeneous Catalysis: Understanding for Designing, and Designing for Applications, *Angew. Chem., Int. Ed.*, 2016, **55**(21), 6112–6113, DOI: 10.1002/anie.201601231.

3 L. Jiao, Y. Wang, H.-L. Jiang and Q. Xu, Metal-Organic Frameworks as Platforms for Catalytic Applications, *Adv. Mater.*, 2018, **30**(37), 1703663.

4 R. Wei, C. A. Gaggioli, G. Li, T. Islamoglu, Z. Zhang, P. Yu, O. K. Farha, C. J. Cramer, L. Gagliardi, D. Yang and B. C. Gates, Tuning the Properties of Zr 6 O 8 Nodes in the Metal Organic Framework UiO-66 by Selection of Node-Bound Ligands and Linkers, *Chem. Mater.*, 2019, **31**(5), 1655–1663.

5 E. A. Dolgopolova, A. J. Brandt, O. A. Ejegbavwo, A. S. Duke, T. D. Maddumapatabandi, R. P. Galhenage, B. W. Larson, O. G. Reid, S. C. Ammal, A. Heyden, M. Chandrashekhar, V. Stavila, D. A. Chen and N. B. Shustova, Electronic Properties of Bimetallic Metal–Organic Frameworks (MOFs): Tailoring the Density of Electronic States through MOF Modularity, *J. Am. Chem. Soc.*, 2017, **139**(14), 5201–5209.

6 A. W. Stubbs, L. Braglia, E. Borfecchia, R. J. Meyer, Y. Román-Leshkov, C. Lamberti and M. Dincă, Selective Catalytic Olefin Epoxidation with Mn II -Exchanged MOF-5, *ACS Catal.*, 2018, **8**(1), 596–601, DOI: 10.1021/acscatal.7b02946.

7 Y. K. Hwang, D. Hong, J. Chang, S. H. Jhung, Y. Seo, J. Kim, A. Vimont, M. Daturi, C. Serre and G. Férey, Amine Grafting on Coordinatively Unsaturated Metal Centers of MOFs: Consequences for Catalysis and Metal Encapsulation. Angew, *Chemie*, 2008, **120**(22), 4212–4216.

8 Z. Fang, B. Bueken, D. E. De Vos and R. A. Fischer, Defect-Engineered Metal-Organic Frameworks, *Angew. Chem., Int. Ed.*, 2015, **54**(25), 7234–7254.

9 D. Hong, Y. K. Hwang, C. Serre, G. Ferey and J. Chang, Porous Chromium Terephthalate MIL-101 with Coordinatively Unsaturated Sites: Surface Functionalization, Encapsulation, Sorption and Catalysis, *Adv. Funct. Mater.*, 2009, **19**(10), 1537–1552.

10 Ü. Kökçam-Demir, A. Goldman, L. Esrafili, M. Gharib, A. Morsali, O. Weingart and C. Janiak, Coordinatively Unsaturated Metal Sites (Open Metal Sites) in Metal–Organic Frameworks: Design and Applications, *Chem. Soc. Rev.*, 2020, **49**(9), 2751–2798.

11 G. C. Shearer, S. Chavan, S. Bordiga, S. Svelle, U. Olsbye and K. P. Lillerud, Defect Engineering: Tuning the Porosity and Composition of the Metal–Organic Framework UiO-66 via Modulated Synthesis, *Chem. Mater.*, 2016, **28**(11), 3749–3761.

12 D. Yang, M. A. Ortuño, V. Bernales, C. J. Cramer, L. Gagliardi and B. C. Gates, Structure and Dynamics of Zr 6 O 8 Metal–Organic Framework Node Surfaces Probed with Ethanol Dehydration as a Catalytic Test Reaction, *J. Am. Chem. Soc.*, 2018, **140**(10), 3751–3759.

13 F. Vermoortele, R. Ameloot, L. Alaerts, R. Matthessen, B. Carlier, E. V. R. Fernandez, J. Gascon, F. Kapteijn and D. E. De Vos, Tuning the Catalytic Performance of Metal–Organic Frameworks in Fine Chemistry by Active Site Engineering, *J. Mater. Chem.*, 2012, **22**(20), 10313.

14 F. G. Cirujano and F. X. Llabrés i Xamena, Tuning the Catalytic Properties of UiO-66 Metal–Organic Frameworks: From Lewis to Defect-Induced Brønsted Acidity, *J. Phys. Chem. Lett.*, 2020, **11**(12), 4879–4890.

15 J. N. Hall and P. Bollini, Metal–Organic Framework MIL-100 Catalyzed Acetalization of Benzaldehyde with Methanol: Lewis or Brønsted Acid Catalysis?, *ACS Catal.*, 2020, **10**(6), 3750–3763.

16 Y. Liu, R. C. Klet, J. T. Hupp and O. Farha, Probing the Correlations between the Defects in Metal–Organic Frameworks and Their Catalytic Activity by an Epoxide Ring-Opening Reaction, *Chem. Commun.*, 2016, **52**(50), 7806–7809.

17 Y. Bai, Y. Dou, L.-H. Xie, W. Rutledge, J.-R. Li and H.-C. Zhou, Zr-Based Metal–Organic Frameworks: Design, Synthesis, Structure, and Applications, *Chem. Soc. Rev.*, 2016, **45**(8), 2327–2367.

18 F. G. Cirujano, MOFs vs. Zeolites: Carbonyl Activation with M (IV) Catalytic Sites, *Catal. Sci. Technol.*, 2017, **7**(23), 5482–5494.

19 S. Rojas-Buzo, P. García-García and A. Corma, Hf-Based Metal–Organic Frameworks as Acid–Base Catalysts for the Transformation of Biomass-Derived Furanic Compounds into Chemicals, *Green Chem.*, 2018, **20**(13), 3081–3091.

20 S. Rojas-Buzo, P. García-García and A. Corma, Zr-MOF-808@MCM-41 Catalyzed Phosgene-Free Synthesis of Polyurethane Precursors, *Catal. Sci. Technol.*, 2019, **9**(1), 146–156.

21 M. H. Beyzavi, R. C. Klet, S. Tussupbayev, J. Borycz, N. A. Vermeulen, C. J. Cramer, J. F. Stoddart, J. T. Hupp and O. K. Farha, A Hafnium-Based Metal–Organic Framework as an Efficient and Multifunctional Catalyst for Facile CO2 Fixation and Regioselective and Enantioretentive Epoxide Activation, *J. Am. Chem. Soc.*, 2014, **136**(45), 15861–15864.

22 V. R. Bakuru, S. R. Churipard, S. P. Maradur and S. B. Kalidindi, Exploring the Brønsted Acidity of UiO-66 (Zr, Ce, Hf) Metal–Organic Frameworks for Efficient Solketal Synthesis from Glycerol Acetalization, *Dalton Trans.*, 2019, **48**(3), 843–847.

23 N. Stock and S. Biswas, Synthesis of Metal-Organic Frameworks (MOFs): Routes to Various MOF Topologies, Morphologies, and Composites, *Chem. Rev.*, 2012, **112**(2), 933–969.

24 Z. Hu, Y. Peng, Z. Kang, Y. Qian and D. Zhao, A Modulated Hydrothermal (MHT) Approach for the Facile Synthesis of UiO-66-Type MOFs, *Inorg. Chem.*, 2015, **54**(10), 4862–4868.

25 Z. Hu, A. Nalaparaju, Y. Peng, J. Jiang and D. Zhao, Modulated Hydrothermal Synthesis of UiO-66 (Hf)-Type Metal–Organic Frameworks for Optimal Carbon Dioxide Separation, *Inorg. Chem.*, 2016, **55**(3), 1134–1141.

26 H. Reinsch, S. Waitschat, S. M. Chavan, K. P. Lillerud and N. Stock, A Facile "Green" Route for Scalable Batch Production and Continuous Synthesis of Zirconium MOFs, *Eur. J. Inorg. Chem.*, 2016, **2016**(27), 4490–4498.

27 Z. Hu, T. Kundu, Y. Wang, Y. Sun, K. Zeng and D. Zhao, Modulated Hydrothermal Synthesis of Highly Stable MOF-808 (Hf) for Methane Storage, *ACS Sustainable Chem. Eng.*, 2020, **8**(46), 17042–17053.

28 N. Van Velthoven, M. Henrion, J. Dallenes, A. Krajnc, A. L. Bugaev, P. Liu, S. Bals, A. V. Soldatov, G. Mali and D. E. S. De Vos, O-Functionalized Metal–Organic Frameworks as Heterogeneous Single-Site Catalysts for the Oxidative Alkenylation of Arenes via C–H Activation, *ACS Catal.*, 2020, **10**(9), 5077–5085.

29 H. Furukawa, F. Gandara, Y.-B. Zhang, J. Jiang, W. L. Queen, M. R. Hudson and O. M. Yaghi, Water Adsorption in Porous Metal–Organic Frameworks and Related Materials, *J. Am. Chem. Soc.*, 2014, **136**(11), 4369–4381.

30 B. Villoria-del-Álamo, S. Rojas-Buzo, P. García-García and A. Corma, Zr-MOF-808 as Catalyst for Amide Esterification, *Chem.–Eur. J.*, 2021, **27**(14), 4588–4598.

31 S. M. Heald, J. O. Cross, D. L. Brewe and R. A. Gordon, The PNC/XOR X-Ray Microprobe Station at APS Sector 20, *Nucl. Instrum. Methods Phys. Res., Sect. A*, 2007, **582**(1), 215–217.

32 B. Ravel and M. Newville, ATHENA, ARTEMIS, HEPHAESTUS: Data Analysis for X-Ray Absorption Spectroscopy Using IFEFFIT, *J. Synchrotron Radiat.*, 2005, **12**(4), 537–541.

33 Y. Zhao and D. G. Truhlar, The M06 Suite of Density Functionals for Main Group Thermochemistry, Thermochemical Kinetics, Noncovalent Interactions, Excited States, and Transition Elements: Two New Functionals and Systematic Testing of Four M06-Class Functionals and 12 Other Function, *Theor. Chem. Acc.*, 2008, **120**(1–3), 215–241.

34 R. Ditchfield, W. J. Hehre and J. A. Pople, Self-Consistent Molecular-Orbital Methods. IX. An Extended Gaussian-Type Basis for Molecular-Orbital Studies of Organic Molecules, *J. Chem. Phys.*, 1971, **54**(2), 724–728.

35 W. J. Hehre, R. Ditchfield and J. A. Pople, Self—Consistent Molecular Orbital Methods. XII. Further Extensions of Gaussian—Type Basis Sets for Use in Molecular Orbital Studies of Organic Molecules, *J. Chem. Phys.*, 1972, **56**(5), 2257–2261.

36 P. J. Hay and W. R. Wadt, Ab Initio Effective Core Potentials for Molecular Calculations. Potentials for the Transition Metal Atoms Sc to Hg, *J. Chem. Phys.*, 1985, **82**(1), 270–283.

37 P. J. Hay and W. R. Wadt, Ab Initio Effective Core Potentials for Molecular Calculations. Potentials for K to Au Including the Outermost Core Orbitals, *J. Chem. Phys.*, 1985, **82**(1), 299–310.

38 M. J. Frisch, G. W. Trucks, H. B. Schlegel, G. E. Scuseria, M. A. Robb, J. R. Cheeseman, G. Scalmani, V. Barone, B. Mennucci, G. A. Petersson, H. Nakatsuji, M. Caricato, X. Li, H. P. Hratchian, A. F. Izmaylov, J. Bloino., G. Zheng and D. J. Sonnenb, No Title, *Gaussian, Inc.*, Wallingford CT, 2009.

39 R. Ditchfield, Self-Consistent Perturbation Theory of Diamagnetism, *Mol. Phys.*, 1974, **27**(4), 789–807.

40 K. Wolinski, J. F. Hinton and P. Pulay, Efficient Implementation of the Gauge-Independent Atomic Orbital Method for NMR Chemical Shift Calculations, *J. Am. Chem. Soc.*, 1990, **112**(23), 8251–8260.

41 S. Rojas-Buzo, A. Corma, M. Boronat and M. Moliner, Unraveling the Reaction Mechanism and Active Sites of Metal–Organic Frameworks for Glucose Transformations in Water: Experimental and Theoretical Studies, *ACS Sustainable Chem. Eng.*, 2020, **8**(43), 16143–16155.

42 E. Plessers, G. Fu, C. Y. Tan, D. E. De Vos and M. B. J. Roeffaers, Zr-Based MOF-808 as Meerwein–Ponndorf–Verley Reduction Catalyst for Challenging Carbonyl Compounds, *Catalysts*, 2016, **6**(7), 104.

43 G. Fu, B. Bueken and D. De Vos, Zr-Metal-Organic Framework Catalysts for Oxidative Desulfurization and Their Improvement by Postsynthetic Ligand Exchange, *Small Methods*, 2018, **2**(12), 1800203.

44 K. Chakarova, I. Strauss, M. Mihaylov, N. Drenchev and K. Hadjiivanov, Evolution of Acid and Basic Sites in UiO-66 and UiO-66-NH2 Metal-Organic Frameworks: FTIR Study by Probe Molecules, *Microporous Mesoporous Mater.*, 2019, **281**, 110–122.

45 J. Jiang, F. Gándara, Y.-B. Zhang, K. Na, O. M. Yaghi and W. G. Klemperer, Superacidity in Sulfated Metal–Organic Framework-808, *J. Am. Chem. Soc.*, 2014, **136**(37), 12844–12847.

46 J. D. Lewis, M. Ha, H. Luo, A. Faucher, V. K. Michaelis and Y. Román-Leshkov, Distinguishing Active Site Identity in Sn-Beta Zeolites Using 31P MAS NMR of Adsorbed

Trimethylphosphine Oxide, *ACS Catal.*, 2018, **8**(4), 3076–3086.

47 C. A. Trickett, T. M. Osborn Popp, J. Su, C. Yan, J. Weisberg, A. Huq, P. Urban, J. Jiang, M. J. Kalmutzki, Q. Liu, J. Baek, M. P. Head-Gordon, G. A. Somorjai, J. A. Reimer and O. M. Yaghi, Identification of the Strong Brønsted Acid Site in a Metal–Organic Framework Solid Acid Catalyst, *Nat. Chem.*, 2019, **11**(2), 170–176.

48 T. J. Matemb Ma Ntep, H. Reinsch, C. Schlüsener, A. Goldman, H. Breitzke, B. Moll, L. Schmolke, G. Buntkowsky and C. Janiak, Acetylenedicarboxylate and In Situ Generated Chlorofumarate-Based Hafnium (IV)–Metal–Organic Frameworks: Synthesis, Structure, and Sorption Properties, *Inorg. Chem.*, 2019, **58**(16), 10965–10973.

49 X. Wang, J. Hao, L. Deng, H. Zhao, Q. Liu, N. Li, R. He, K. Zhi and H. Zhou, The Construction of Novel and Efficient Hafnium Catalysts Using Naturally Existing Tannic Acid for Meerwein–Ponndorf–Verley Reduction, *RSC Adv.*, 2020, **10**(12), 6944–6952.

50 L. Botti, S. A. Kondrat, R. Navar, D. Padovan, J. S. Martinez-Espin, S. Meier and C. Hammond, Solvent-Activated Hafnium-Containing Zeolites Enable Selective and Continuous Glucose–Fructose Isomerisation, *Angew. Chem., Int. Ed.*, 2020, **59**(45), 20017–20023.

51 J. Morais, L. Miotti, K. P. Bastos, S. R. Teixeira, I. J. R. Baumvol, A. L. P. Rotondaro, J. J. Chambers, M. R. Visokay, L. Colombo and M. C. M. Alves, Environment of Hafnium and Silicon in Hf-Based Dielectric Films: An Atomistic Study by X-Ray Absorption Spectroscopy and x-Ray Diffraction, *Appl. Phys. Lett.*, 2005, **86**(21), 212906.

52 D. Gianolio, J. G. Vitillo, B. Civalleri, S. Bordiga, U. Olsbye, K. P. Lillerud, L. Valenzano and C. Lamberti, Combined Study of Structural Properties on Metal-Organic Frameworks with Same Topology but Different Linkers or Metal, *J. Phys.: Conf. Ser.*, 2013, **430**, 012134.

53 S. Rojas-Buzo, P. García-García and A. Corma, Catalytic Transfer Hydrogenation of Biomass-Derived Carbonyls over Hafnium-Based Metal–Organic Frameworks, *ChemSusChem*, 2018, **11**(2), 432–438.

54 Y. Lin, Q. Bu, J. Xu, X. Liu, X. Zhang, G.-P. Lu and B. Zhou, Hf-MOF Catalyzed Meerwein–Ponndorf–Verley (MPV) Reduction Reaction: Insight into Reaction Mechanism, *Mol. Catal.*, 2021, **502**, 111405.

55 Z. Hu, Y. Wang and D. Zhao, The Chemistry and Applications of Hafnium and Cerium (Iv) Metal–Organic Frameworks, *Chem. Soc. Rev.*, 2021, **50**, 4629–4683.

56 J. F. Blandez, A. Santiago-Portillo, S. Navalón, M. Giménez-Marqués, M. Álvaro, P. Horcajada and H. García, Influence of Functionalization of Terephthalate Linker on the Catalytic Activity of UiO-66 for Epoxide Ring Opening, *J. Mol. Catal. A: Chem.*, 2016, **425**, 332–339.

57 P. García-García and A. Corma, Hf-based Metal-Organic Frameworks in Heterogeneous Catalysis, *Isr. J. Chem.*, 2018, **58**(9–10), 1062–1074.

58 P. J. Kunkeler, J. C. van der Waal, J. Bremmer, B. J. Zuurdeeg, R. S. Downing and H. Van Bekkum, Application of Zeolite Titanium Beta in the Rearrangement of α-Pinene Oxide to Campholenic Aldehyde. Catal, *Letters*, 1998, **53**(1), 135–138.

59 A. Corma and H. García, Lewis Acids: From Conventional Homogeneous to Green Homogeneous and Heterogeneous Catalysis, *Chem. Rev.*, 2003, **103**(11), 4307–4366.

60 M. Stekrova, N. Kumar, A. Aho, I. Sinev, W. Gruenert, J. Dahl, J. Roine, S. S. Arzumanov, P. Mäki-Arvela and D. Y. Murzin, Isomerization of α-Pinene Oxide Using Fe-Supported Catalysts: Selective Synthesis of Campholenic Aldehyde, *Appl. Catal., A*, 2014, **470**, 162–176.

61 J. Jiang and O. M. Yaghi, Brønsted Acidity in Metal–Organic Frameworks, *Chem. Rev.*, 2015, **115**(14), 6966–6997.

62 X. Feng, J. Hajek, H. S. Jena, G. Wang, S. K. P. Veerapandian, R. Morent, N. De Geyter, K. Leyssens, A. E. J. Hoffman and V. Meynen, Engineering a Highly Defective Stable UiO-66 with Tunable Lewis-Brønsted Acidity: The Role of the Hemilabile Linker, *J. Am. Chem. Soc.*, 2020, **142**(6), 3174–3183.